Available online at www.sciencedirect.com
SCIENCE DIRECT®
ELSEVIER
Nuclear Instruments and Methods in Physics Research A 519 (2004) 425–431
NUCLEAR INSTRUMENTS & METHODS IN PHYSICS RESEARCH Section A
www.elsevier.com/locate/nima

Beam-halo in mismatched proton beams

T.P. Wangler[a,*], C. K. Allen[a], K.C.D. Chan[a], P.L. Colestock[a], K.R. Crandall[b], R.W. Garnett[a], J.D. Gilpatrick[a], W. Lysenko[a], J. Qiang[c], J.D. Schneider[a], M.E. Schulze[d], R.L. Sheffield[a], H.V. Smith[a]

[a] *Los Alamos National Laboratory, Los Alamos, NM 87544, USA*
[b] *TechSource, Santa Fe, NM 87594-1057, USA*
[c] *Lawrence Berkeley National Laboratory, Berkeley, CA 94720, USA*
[d] *General Atomics, Los Alamos, NM 87545, USA*

Abstract

Progress was made during the past decade towards a better understanding of halo formation caused by beam mismatch in high-intensity beams. To test these ideas an experiment was carried out at Los Alamos with proton beams in a 52-quadrupole focusing channel. Rms emittances and beam widths were obtained from measured beam profiles for comparison with the maximum emittance-growth predictions of a free-energy model and the maximum halo-amplitude predictions of a particle-core model. The experimental results are also compared with multiparticle simulations. In this paper we will present the experimental results and discuss the implications with respect to the validity of both the models and the simulations.

PACS: 29.17.+w; 29.27.Bd; 41.75.−i; 41.85.Ew

Keywords: Beam halo; Emittance growth; Beam profiles; Simulations; Space charge; Mismatch

1. Introduction

Control of beam-halo and associated beam losses is a fundamental requirement for high beam availability in high-power proton linacs. More than a decade ago, computer simulation studies [1] identified beam mismatch as the major source of the halo and emittance growth observed in simulations. The emittance growth can be related to the conversion of free-energy from mismatch oscillations into thermal energy of the beam. For a given mismatch strength, the free-energy model determines the maximum emittance growth, which results from complete transfer of free-energy into emittance [2].

A physical model of halo formation is expected to include both nonlinear and time-dependent forces that drive halo particles to larger amplitudes. Such a mechanism is provided by the particle-core model [3,4,5], in which beam mismatch produces an imbalance between focusing, space charge, and emittance, exciting a symmetric or breathing (x_{rms} and y_{rms} in-phase) mode oscillation of the core. The space-charge field of the oscillating core modulates the net focusing force acting on individual particles and drives particles in a nonlinear parametric resonance when

*Corresponding author..
E-mail address: twangler@lanl.gov (T.P. Wangler).

0168-9002/$ - see front matter © 2003 Elsevier B.V. All rights reserved.
doi:10.1016/j.nima.2003.11.182

$f_{particle} = f_{mode}/2$, where $f_{particle}$ is the betatron frequency of the particle and f_{mode} is the mode-oscillation frequency [4]. The model predicts a maximum resonant-particle amplitude as a function of the mismatch strength [5]. Neither the free-energy, nor the particle-core model predict the growth rates for the halo amplitude and beam emittance, for which numerical simulations are required.

2. Beam-halo experiment

To test the two models, we installed a 52-quadrupole periodic-focusing beam-transport channel at the end of the Los Alamos low-energy demonstration accelerator (LEDA)[6]. LEDA delivers a 6.7-MeV proton beam from a 350-MHz radiofrequency-quadrupole (RFQ) linac. The beam was pulsed at a 1-Hz rate with a 30-μs pulse length. The channel length of 11 m was sufficient for the development of about 10 mismatch oscillations, enough to observe at least the initial stages of emittance growth and halo formation caused by mismatch. In this paper we present results for a 75-mA proton beam current.

The most important beam-diagnostic elements were the transverse beam-profile scanners [7] that measured the horizontal and vertical distributions. These were installed at nine stations (Fig. 1), each located midway between pairs of quadrupoles. The scanners were labeled with numbers corresponding to the preceding quadrupole-magnet number. The beam was matched, using a least-squares fitting procedure that adjusted the first four quadrupoles to produce equal rms sizes at the last eight scanner locations. For a mismatched beam one must consider not only the breathing mode, but also the antisymmetric or quadrupole mode. The beam was mismatched in nominally pure symmetric or antisymmetric modes by proper settings of the same four matching quadrupoles. More details of the matching and mismatching procedures can be found in Ref [8]. The mismatch strength was measured by a mismatch parameter μ, which equals the ratio of the rms size of the initial beam to that of the matched beam. For a matched beam $\mu = 1$.

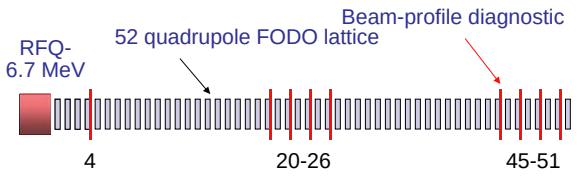

Fig. 1. Block diagram of the 52-quadrupole-magnet lattice showing the nine locations of beam-profile scanners.

Fig. 2 shows the matched and mismatched 75-mA beam profiles at scanner 51. The matched beam has a Gaussian-like central profile with an rms beam size of 1.1 mm. For the matched beam a low-density halo is observed to extend as far as 9 rms. This matched-beam halo is observed at all scanners and is most easily explained as a halo that has formed in the injector/RFQ system prior to the periodic quadrupole channel. Direct measurement of the beam-energy distribution with a resolution of about 200 keV, using a dispersive section of the transport line at the end of the periodic quadrupole channel, showed no evidence for low-energy tails that might contribute to this halo. Although collimation can remove this halo, collimation was not implemented in our experiment. Halo caused by mismatch was our main interest, because this mismatch mechanism is expected to involve more particles, and can form halo even at high energy where collimation is more difficult. A breathing-mode-mismatch beam profile for $\mu = 1.5$, seen in Fig. 2, shows the growth of shoulders indicating substantial formation of halo.

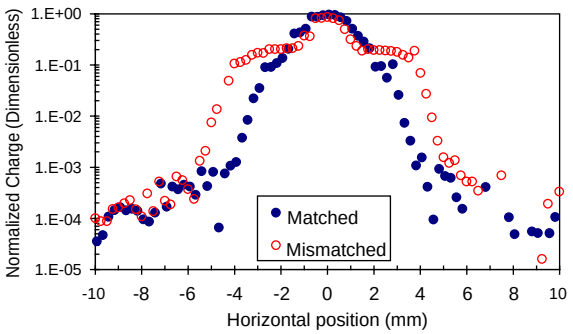

Fig. 2. Horizontal beam profiles at scanner 51 for a 75-mA, $\mu = 1$ matched beam (blue solid circles), and breathing-mode $\mu = 1.5$ mismatched beam (red open circles).

The rms-size measurements were used to calculate the rms emittances at scanners 20 and 45 [6]. Assuming zero emittance growth in the channel for the matched beam, the tune depression from space-charge was 0.82 immediately after the matching quadrupoles at scanner 4, and was constant at 0.95 after the beam had debunched at approximately quadrupole 16, about 3.5 m from the beginning of the channel. Although the beam was not in a space-charge-dominated regime, significant space-charge effects in mismatched beams were still expected.

The free-energy model can be tested by comparing the measured emittance-growths at scanners 20 and 45 with the emittance-growth upper limits from that model. The emittance-growth measurements for mismatched beams show some significant anisotropies (x–y differences). Franchetti et al. [9] report simulation studies of anisotropic beams in uniform focusing channels, in which large (40%) x–y emittance-growth differences are observed that are sensitive to initial x–y tune differences as small as 1%. The sensitivity is not the result of chaotic behavior, but is caused by the parametric resonance discussed earlier, which is sensitive to x–y parameter differences. In our case, anisotropies could be driven by percent-level input x–y emittance differences that are not resolved experimentally. Although the free-energy model was derived for an axisymmetric beam, these authors find that the model can be extended to a 2D anisotropic case if the emittance growth is averaged over x and y.

Fig. 3 shows the x–y averaged rms-emittance-growth results (points with error bars) versus μ at scanner 20 for a 75-mA breathing-mode mismatch. The maximum emittance-growth curves from the free-energy model are shown for the two tune-depression values that bracket the values for the debunching beam, and it can be seen that the theoretical maximum is insensitive to the tune depression over this range. The breathing-mode data in Fig. 3 are consistent at all μ values with the maximum emittance growth predicted by the model. The breathing mode results at scanner 45 (not shown) show no significant additional emittance growth, consistent with the upper limits from the model and with complete transfer of free energy within only four mismatch oscillations. Quadrupole mismatch data at 75 mA are not available at scanner 20, but are available at scanner 45 (see Fig. 4). These results are also consistent at all measured μ values with the maximum growth of the model. Although an axisymmetric beam is assumed in the model, applicability to the quadruple mode is physically reasonable for a given free energy if equal energy sharing is assumed in x and y. Overall, the data for both mismatch modes indicate a rapid growth mechanism with nearly complete transfer of free energy occurring in less than 10 mismatch oscillations.

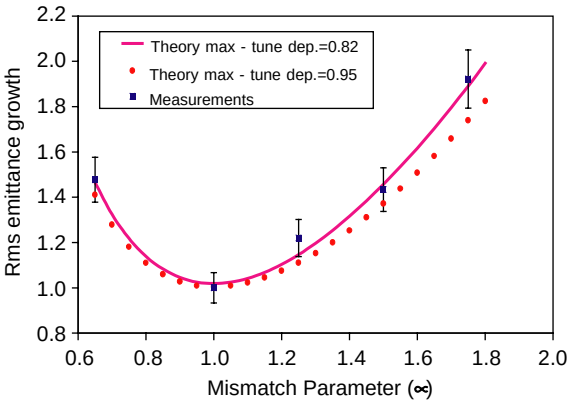

Fig. 3. Measured rms-emittance growth averaged over x and y for 75 mA at scanner 20 for a breathing-mode mismatch. The curves show maximum growth from the free-energy model.

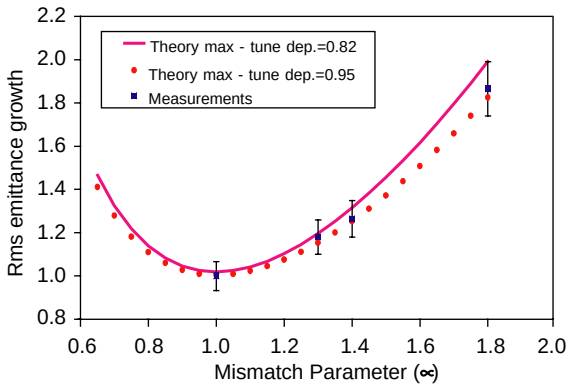

Fig. 4. Measured rms-emittance growth averaged over x and y for 75 mA at scanner 45 for a quadrupole-mode mismatch. The curves show maximum growth from the free-energy model.

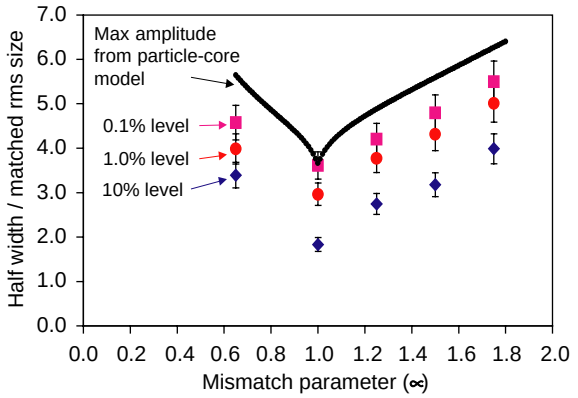

Fig. 5. Measured beam half-widths at scanner 20 (75 mA and a breathing mode mismatch) at different fractional intensity levels versus mismatch strength μ for comparison with the maximum resonant amplitude of the particle-core model.

The particle-core model predicts the maximum resonant-particle amplitude as a function of mismatch parameter μ [5]. We were unable to determine an experimental maximum amplitude for direct comparison because of background. Instead, we compared the measured amplitudes (x–y averaged half-widths of the beam) at three different fractional beam-profile intensity levels (10%, 1%, and 0.1% of the peak) for a breathing-mode mismatch with the maximum amplitude predicted by the particle-core model. A comparison is shown in Fig. 5 for scanner 20 at 75 mA. The shapes of all three measured half-width curves are consistent with the shape of the maximum amplitude curve from the particle-core model, and all three measured curves lie below the maximum amplitude curve from the model. Similar results are observed at scanner 51. Although the particle-core model based on a single mismatch mode is a relatively simple description of the beam dynamics, the agreement with the model for the curve shapes and for the consistency of the magnitudes, supports the conclusion that the model incorporates the main physical mechanism responsible for the halo growth.

3. Multiparticle simulations

Self-consistent multiparticle simulations including space-charge forces were carried out using the macroparticle simulation code IMPACT [10]. The lack of detailed knowledge of the initial beam distribution in phase space is an important issue for the simulations. Our first approach has been to generate three different initial distributions at the entrance of the beam-transport channel, all with the same Courant–Snyder ellipse parameters and emittances; the latter were deduced from the measurements. The three input distributions are: (1) 6D Waterbag, (2) 6D Gaussian, and (3) a distribution called LEBT/RFQ, generated from a simulation through the LEBT and RFQ, starting at the plasma surface at the exit of the ion source. The particle coordinates of the LEBT/RFQ distribution were scaled to produce the correct initial Courant–Snyder parameters and emittances. The transverse phase-space plots of these distributions are shown in Fig. 6. Fig. 6 shows qualitatively an increasing input beam halo as we progress from the Waterbag to the Gaussian to the LEBT/RFQ distribution. For each of these initial distributions we have simulated the beam dynamics through the matched beam channel [11,12]. For each simulation, using about 2.8 million macroparticles with a computation grid of $65 \times 65 \times 129$, Poisson's equation was solved in cylindrical coordinates with transverse perfect-conducting-wall boundary conditions and a periodic boundary condition, longitudinally.

All three initial distributions predict a nearly matched transverse rms beam size, in good agreement with the matched-beam measurements. In addition to the rms sizes, we also measured the projected density distributions, i.e. beam profiles in x and y at nine locations along the transport channel. The density profiles from the simulations of the matched beam are compared in Fig. 7 with measurements at the final detector. In general, the LEBT/RFQ simulation agrees best with the measured profiles, especially in the core region. However, none of the distributions reproduce well the tails observed in the measured profiles.

Fig. 8 shows the horizontal-profile comparison at the final detector, for the LEBT/RFQ simulation and for a breathing-mode mismatch with an initial rms beam size that is 50% larger than the matched case. Simulations for all three initial distributions fail to reproduce the broad shoulders

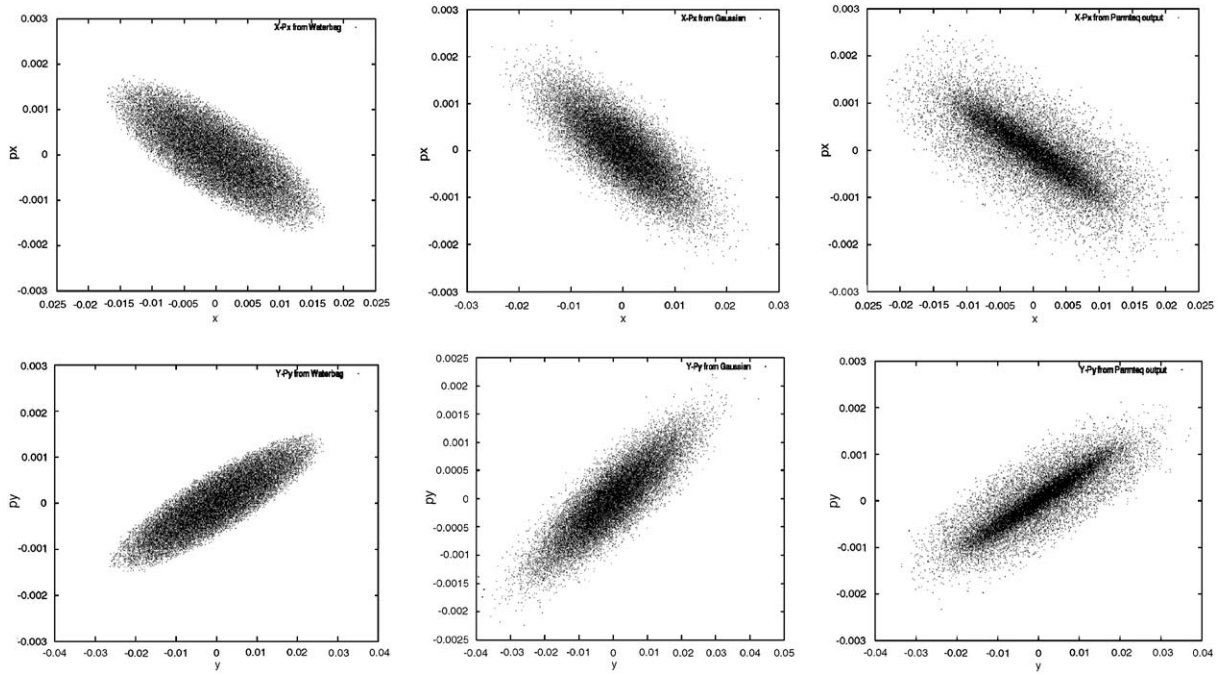

Fig. 6. Transverse phase-space projections for three initial simulation distributions at the entrance of the transport channel for the matched beam: 6D Waterbag (left), 6D Gaussian (middle), and RFQ/LEBT (right). The upper plots show $x - p_x$ phase space, and the lower plots show $y - p_y$ phase space.

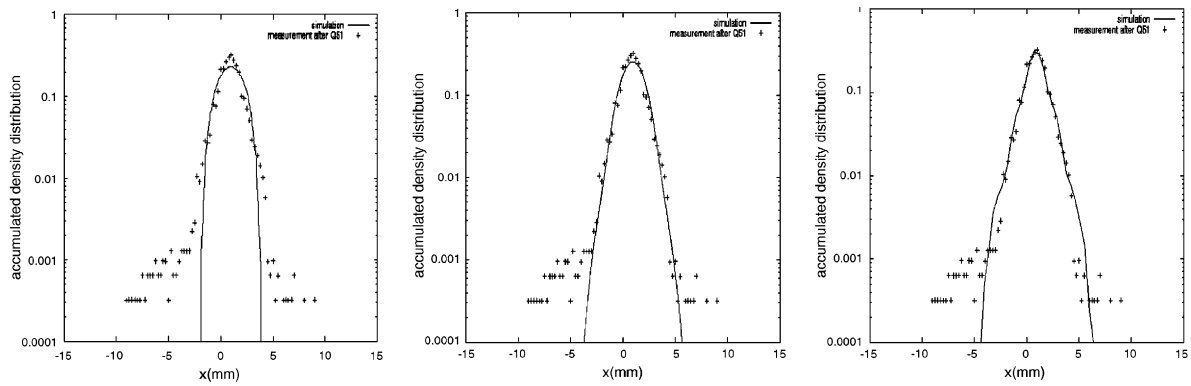

Fig. 7. Horizontal profiles from measurements (points) and simulations (curves) at the final profile detector for 75-mA matched beam. The initial distributions for the simulations are: 6D Waterbag (left), 6D Gaussian (center), and LEBT/RFQ (right).

seen in Fig. 8, which are induced in the measured beam profiles by the mismatches. The broader shoulders for the real beam are evidence of a more rapid halo growth rate in the real mismatched beam than in the simulations.

Fig. 9 compares the rms emittance growth at the end of the channel calculated from the measurements at 75 mA for the breathing-mode mismatched beam (initial rms size 50% larger than the matched size) with those from the three simulations. We find that the emittance-growth rates from simulations increase as we progress from the 6D Waterbag to 6D Gaussian to the LEBT/RFQ distribution, which means that the

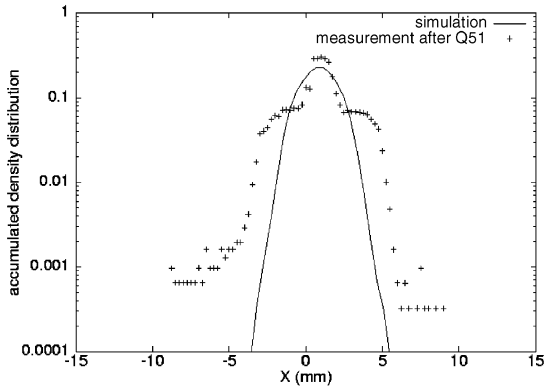

Fig. 8. Horizontal profile from measurements (points) and the LEBT/RFQ simulation (curve) at the final profile detector for a 75-mA breathing-mode mismatched (by 50%) beam.

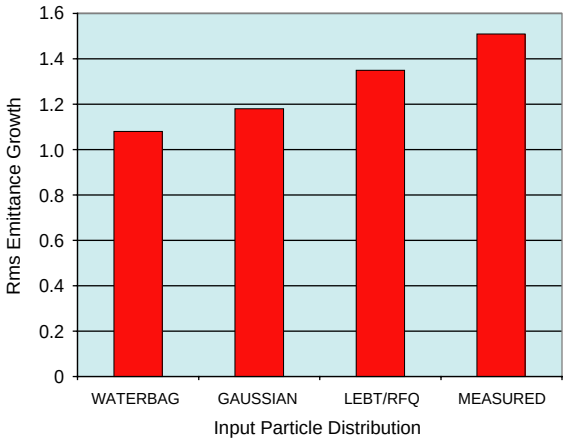

Fig. 9. Emittance growth from three simulations and from the experiment, for a 50% breathing-mode mismatch at 75 mA.

distributions with greater initial beam-halo have more emittance growth. We interpret this as a result that would be expected from the particle-core model [5], because the resonant particles that form the halo lie outside the beam core. The emittance-growth rate calculated from measurements is larger than those from any of the three simulations. Our interpretation is that the initial distributions assumed for the simulations do not adequately populate the tails, which include the resonant particles that are main source of the halo and emittance growth.

As a further test of the hypothesis that the emittance growth is enhanced by the population of the tail of the input beam, we have done simulations for 75 mA and a $\mu = 1.5$ mismatch, using a distribution that is the sum of two Gaussians with different relative heights and different rms sizes. Choosing a fixed ratio of the rms widths of the two Gaussian distributions equal to 4, we find that as the height of the broader Gaussian, which provides the tails, increases relative to the height of the narrower one from 5% to 20%, the simulated emittance growth increases from 1.20 to 1.47. We note that the emittance-growth value of 1.47 lies within the experimental uncertainly of the measured value of 1.51. This example confirms that an emittance growth of the approximate magnitude of the measured result can be obtained from simulation, by using an initial distribution with a large population in the tail. For the mismatched beam profiles, we observe broader shoulders in simulations using the double-Gaussian initial distribution than for the previous three distributions. However, these simulation profiles still do not reproduce well the density profiles from the measurements (see Fig. 10). We believe that more experimental information about the initial distribution would be required to reproduce the details of the measured mismatched density profiles.

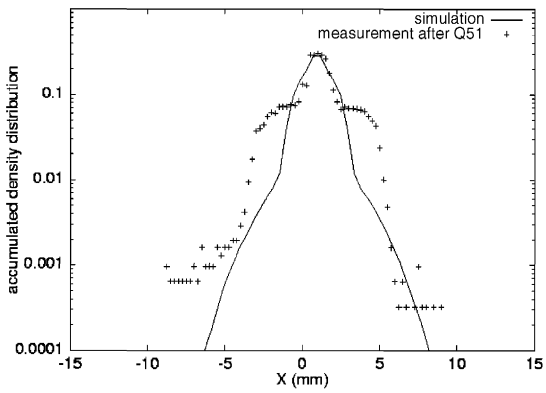

Fig. 10. Horizontal profile from measurements (points) and simulation for an initial double-Gaussian with relative heights of 20% simulation (curve) at the final profile detector for a 75-mA breathing-mode mismatched (by 50%) beam.

4. Conclusions

Our experimental results support both the free-energy model and the particle-core model of halo formation in mismatched beams. This conclusion is important because these models predict upper limits to emittance and halo-amplitude growth in high-current transport channels and linacs, and allow estimation of focusing strength and aperture requirements in new designs. We also conclude that using only the known Courant–Snyder parameters and the emittances as input parameters is not sufficient information for reliable simulations of beam halo formed in mismatched beams. Our interpretation of the simulation results is that the higher emittance-growth rate for the real beam is caused by a higher particle density in the initial beam tails, and consequently, a greater population of the region of phase space that leads to resonant halo growth. We conclude that knowledge of the initial particle distribution, especially the density in the tails, is important for accurate predictions of the beam profiles beam-halo from simulations.

Acknowledgements

We thank the dedicated LEDA personnel who made the experiment possible. We thank Ingo Hofmann for sending a draft of his paper on anisotropy effects in mismatched beams, which helped us to interpret our results. We thank Lloyd Young for providing a multiparticle simulation used to generate one of our input beams. We thank Martin Reiser, Ingo Hofmann, Jerry Nolen, Pat O'Shea, and Irving Haber for helpful conversations. This work was supported by the US Department of Energy. Simulations in this research were performed in part using resources of the National Energy Research Scientific Computing Center, which is supported by the Office of Science of the US Department of Energy.

References

[1] A. Cucchetti, et al., Proceedings of IEEE 1991 Particle Accelerator Conference, Lizama and Chew (Eds.), IEEE, New York, 1991, p. 251.
[2] M. Reiser, Theory and Design of Charged Particle Beams, Wiley, New York, 1994, p. 477;
M. Reiser, J. Appl. Phys. 70 (1991) 1919.
[3] J.S. O'Connell, T.P. Wangler, R.S. Mills, K.R. Crandall, Proceedings of 1993 Particle Accelerator Conference, Washington, D.C. IEEE Catalog No. CH3279-7, 493, pp. 3657–3659.
[4] R.L. Gluckstern, Phys. Rev. Lett. 73 (1994) 1247.
[5] T.P. Wangler, K.R. Crandall, R. Ryne, T.S. Wang, Phys. Rev. ST-AB 1 (1998) (084201).
[6] C.K. Allen, et al., Phys. Rev. Lett. 89 (2002) 214802.
[7] J.D. Gilpatrick, et al., Proceedings of 2001 Particle Accelerator Conference, Chicago, IL, IEEE Catalog No. 01CH37268, 2001, pp. 525–527.
[8] T.P. Wangler, LEDA beam halo experiment—physics and concept of the experiment, Los Alamos Report LA-UR-00-3181, July 24, 2000, pp. 13, 14.
[9] G. Franchetti, I. Hofmann, D. Jeon, Phys. Rev. Lett. 88 (2002) 254802.
[10] J. Qiang, R.D. Ryne, S. Habib, V. Decyk, J. Comput. Phys. 163 (2000) 434.
[11] Ji Qiang, et al., Phys. Rev. ST-Accel. Beams 5 (2002) 124201.
[12] T.P. Wangler, Ji Qiang, Los Alamos beam halo experiment: comparing theory, simulation, and experiment, Advanced Accelerator Concepts Workshop, Mandalay Beach, CA, June 22–28, 2002, AIP Conference Proceedings 647, pp. 878–883.